Nanoscale

COMMUNICATION

View Article Online
View Journal | View Issue

Cite this: *Nanoscale*, 2021, **13**, 9553

Received 1st January 2021,
Accepted 16th April 2021

DOI: 10.1039/d1nr00001b

rsc.li/nanoscale

Hydrocarbon contamination in angström-scale channels†

Ravalika Sajja,‡[a,b] Yi You,‡[a,b] Rongrong Qi,[a,b] Solleti Goutham,[a,b] Ankit Bhardwaj,[a,b] Alexander Rakowski,[c] Sarah Haigh,[c] Ashok Keerthi[b,d] and Boya Radha *[a,b]

Nonspecific molecular adsorption such as airborne contamination occurs on most surfaces including those of 2D materials and alters their properties. While surface contamination is studied using a plethora of techniques, the effect of contamination on confined systems such as nanochannels/pores leading to their clogging is still lacking. We report a systematic investigation of hydrocarbon adsorption in angstrom (Å) slit channels of varying heights. Hexane is chosen to mimic the hydrocarbon contamination and the clogging of the Å-channels is evaluated *via* a helium gas flow measurement. The level of hexane adsorption, in other words, the degree of clogging depends on the size difference between the channels and hexane. A dynamic transition of the clogging and revival process is shown in sub-2 nm thin channels. Long-term storage and stability of our Å-channels are demonstrated here for up to three years, alleviating the contamination and unclogging the channels using thermal treatment. This study highlights the importance of the nanochannels' stability and demonstrates the self-cleansing nature of sub-2 nm thin channels enabling a robust platform for molecular transport and separation studies. We provide a method to assess the cleanliness of nanoporous membranes, which is vital for the practical applications of nanofluidics in various fields such as molecular sensing, separation and power generation.

Introduction

Nanopores and nanochannels play an important role both in fundamental studies of confined molecular transport[1] and mimicking biological channels, as well as in applications of molecular and ion sieving membranes,[2] sensors for biomolecular translocation,[3] power generation,[4] gas separation[5] and storage.[6] Some of the well-studied nanochannel systems include carbon nanotubes,[7,8] two-dimensional (2D) laminates such as graphene oxide,[9] clays,[10] MXenes,[11] and quasi-zero dimensional pores such as atomic vacancies,[12] nanopores punctured through 2D-materials,[4,13] to name a few. As much as the pore size is a critical factor in molecular transport for such systems,[14] the influence of the nanochannel surface also becomes significant in mass transport when the pore is of sub-nanometre size, which is comparable to the length scales of molecular interactions.[15]

Often, the surfaces, especially those of 2D-materials, have high surface energy and inevitably adsorb unwanted molecules, resulting in the alteration of their properties.[16] For a long time, it was believed that graphite is hydrophobic as several measurements yielded water contact angles[17] around 90°. Li *et al.*[18] reported the contact angle for freshly prepared graphene to be 44°, which increased to 80° after exposure to ambient atmosphere for a day. This change in graphene hydrophilicity was hypothesized to be caused by physisorption or chemisorption of the molecules (*e.g.* hydrocarbons) from the ambient environment.[19] Such aging related contamination has also been found on other 2D materials such as MoS_2, WS_2 and InSe.[20,21] The nature of the surface contamination on graphene was detailed by placing a layer of hexagonal boron nitride (hBN) on top, so that the contamination could be segregated into pockets due to the self-cleansing nature of 2D materials. These contamination pockets were examined by nanoindentation[22] as well as by cross-sectional transmission electron microscopy[23] to confirm that it is mainly composed of hydrocarbons. Even though the airborne hydrocarbon concentration is very low, ranging from parts per trillion to parts per

[a]*Department of Physics and Astronomy, School of Natural Sciences, The University of Manchester, Oxford Road, Manchester M13 9PL, UK.*
E-mail: radha.boya@manchester.ac.uk
[b]*National Graphene Institute, The University of Manchester, Oxford Road, Manchester M13 9PL, UK*
[c]*Department of Materials, School of Natural Sciences, The University of Manchester, Oxford Road, Manchester M13 9PL, UK*
[d]*Department of Chemistry, School of Natural Sciences, The University of Manchester, Oxford Road, Manchester M13 9PL, UK*

†Electronic supplementary information (ESI) available. See DOI: 10.1039/d1nr00001b

‡These authors contributed equally.

million (ppm),[18] the alteration of the 2D materials' surface is prominent such as the variation of local carrier concentration[16] and change in surface property from hydrophilic to hydrophobic.[18] Several methods have been reported to drive off the contamination from 2D-material surfaces, such as dry cleaning using activated charcoal,[24] thermal annealing[25] and polymer degradation using metal catalysts.[26]

Basal planes of 2D-materials favour hydrocarbon adsorption, and nanochannels/pores pose a further challenging scenario as their edges are highly energetic and are decorated with functional groups; however, only a few reports address hydrocarbon contamination in nanochannels.[27] A systematic study of the contaminants' impact on the nanochannels is essential, particularly to assess their stability and performance in the long run. Various techniques, such as ambient pressure X-ray photoelectron spectroscopy, tip-enhanced infrared spectroscopy, atomic force microscopy, and ellipsometry measurements, are used to characterise hydrocarbon contamination on surfaces.[28–31] However, those methods require a sufficient concentration of hydrocarbons to be able to characterize, whereas the contaminants in the nanochannels are far less and may be buried inside the channel limiting their access. Nevertheless, few attempts have been made to study hydrocarbons under confinement, *e.g.*, imaging of the passage of alkyl and alkenyl fullerenes inside a nanotube was performed using a transmission electron microscope[32] and it was observed that imaging beam can itself cause changes in the hydrocarbons or activate free-radicals.[32,33] Capillary condensation of hexane has been studied inside sub-10 nm pores, where phase changes leading to confinement induced vapor pressure elevation were observed.[34] Selective filling of hexane inside single walled carbon nanotubes was demonstrated,[35] despite the diameter of the nanotubes being smaller than the kinetic diameter of hexane. Apart from the atmospheric contaminants, the flow of fluids in confined channels can be altered by other contaminants such as polymeric residues arising from fabrication processes and by amorphous carbon deposits when using chemically synthesized 2D materials.[36,37]

Here we report gas flow measurements through channels made with angstrom-scale precision as a simple and easy way to track hydrocarbon contamination under confinement. The channel surfaces are made from 2D materials serving as an ideal platform to understand hydrocarbon induced clogging or degradation pertaining to 2D material systems. We use the helium gas flow measurement technique to check the airborne as well as deliberate hydrocarbon contamination using a model hydrocarbon, hexane.

Results and discussion

In this work, we used slit-like channels of various heights ranging from ~0.4 nm to ~11 nm, fabricated from 2D materials namely graphene and hBN. The fabrication recipe is described in our previous reports where we explored the ultrafast water flows and specular gas reflections off the surface of the walls.[37,38] The slit-like channels are akin to a sandwich of three 2D crystals, named the bottom layer, spacer, and top layer, and these channels are assembled over a free-standing silicon nitride (SiN_x) membrane. A schematic of an Å-slit channel is illustrated in Fig. 1a and a detailed fabrication procedure is presented in Fig. S1.† Briefly, the bottom layer (~50 nm thick) and the top layer (~200 nm) are mechanically exfoliated from the high-quality graphite or hBN crystals. The spacer layer is made from a thin layer of graphene which is cut out into parallel strips by electron beam lithography and plasma etching. The bottom and top layers define the channel walls. The distance between the spacer strips and the thickness of the spacer layer determines the channel's width and height respectively. The channel height h can be varied in multiples of numbers of layers N of graphene spacer (shown in the bottom inset of Fig. 1a). For example, a single layer graphene spacer ($N = 1$) means a ~0.4 nm thick channel and a five-layer graphene spacer ($N = 5$) corresponds to a ~1.7 nm-thick channel. A cross-sectional image of a five-layer graphene slit is shown in Fig. 1b, where the individual layers of top and bottom atomically flat graphite crystals are clearly seen.

During and after the fabrication, the channels are susceptible to polymeric and hydrocarbon contamination when stored under ambient conditions. Self-cleansing in sub-2 nm channels leads to such polymeric residues (usually ~1.5 to 2 nm) being squeezed out leaving cleaner channels, as examined in our previous study.[37] However, smaller hydrocarbon molecules can lead to channel clogging and degradation. We assess this *via* helium (He) gas flow measurement through the channels in a vacuum. In the measurement setup (details in Fig. S2†), He gas is input on one side of the device, whereas in the other chamber facing the exit of the channels, the output He is continuously quantified using a mass spectrometer. We monitor the gas flow rate for a given pressure difference and use it as an indicator of the channels' contamination level.

Airborne contamination on Å-slit channels

We first examined the clogging of a freshly fabricated device (Fig. 1c and d) with channels of height $h \sim 1.7$ nm (5-layer graphene spacer). The channels exhibit a noticeable reduction of helium permeance when the device was stored in an ambient environment for 10 days, indicating partial clogging. The degree of clogging was further exacerbated after an ambient air exposure of 20 days. Annealing is commonly used to decontaminate the graphitic carbon substrates as the fouled hydrocarbons are weakly bound through physisorption.[39,40] It was found that upon annealing at a high temperature (400 °C for 5 hours) in a H_2/Ar atmosphere, the channels can be unclogged, and the (pristine state) flow can be recovered. Activated charcoal acts as a contamination sink and a good hydrocarbon adsorbent, as reported for dry cleaning of pristine graphene samples.[24] Hence, after annealing, we stored the same device in charcoal for ~50 days. A helium leak reduction of only ~30% suggests that indeed the observed clogging of channels is most likely due to the airborne hydrocarbon adsorption from the ambient environment.

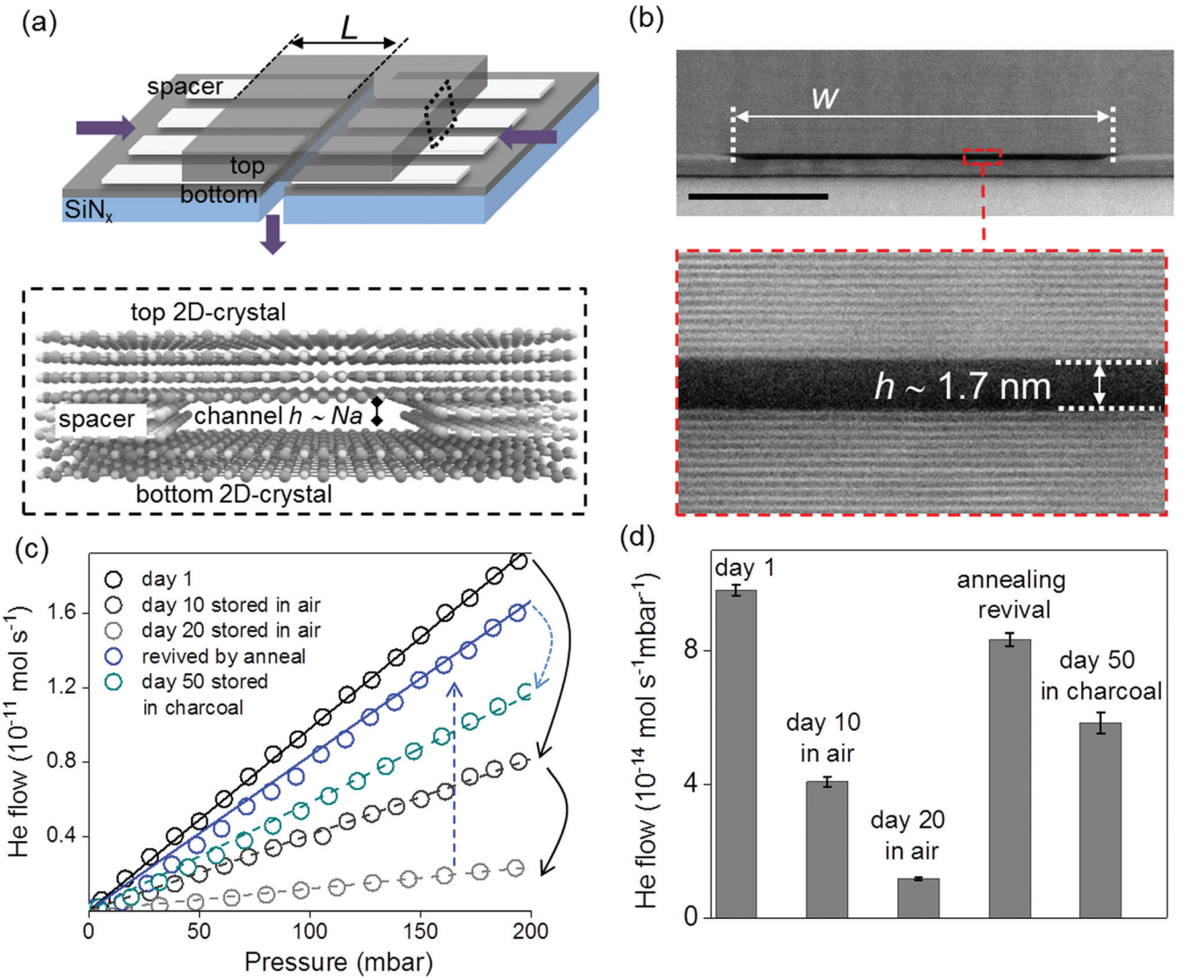

Fig. 1 Airborne contamination in Å-channels. (a) Schematic of a device showing a silicon nitride (SiN_x) membrane with angstrom slit channels on top and their length *L* is noted. Purple arrows indicate the flow directions of the gas through the device. The below inset shows a schematic representation of a channel displaying the top, bottom and spacer layers, with channel height *h* labelled. *N* is the number of layers of graphene spacer, and *a* is the interlayer distance in graphite. (b) Cross-sectional TEM dark field image of a 5-layer channel, with a magnified view shown below. Horizontal bright lines represent individual layers of graphite, and the dark space is the Å-channel. Scale bar of the top image, 50 nm. (c) Helium flow through Å-channels made with a 5-layer graphene spacer (height, $h \sim 1.7$ nm), top and bottom graphite walls. The channels are ~5 μm long, and there were ~200 channels in the device. (d) Bar graph showing the data in (c) for the Å-channel device clogging and revival. Upon storage under ambient conditions, the flow reduced within a few days, probably due to the channel clogging. However, the flow can be regained by annealing at high temperature. Storage in charcoal displayed a minimal flow reduction over ~50 days.

To verify if the hydrocarbon contamination commonly exists in other channels of different thicknesses, we performed the helium leak test as above, on devices with 3-layer and 32-layer channels, respectively. The gas permeability plots in Fig. 2 demonstrate that the extent of the clogging is not similar for these two devices. Specifically, the 3-layer device ($h \sim 1$ nm) displayed ~50% of the He flow reduction, whereas the 32-layer device ($h \sim 11$ nm) showed more than >97% reduction in the permeation and only a minor revival was seen upon thermal treatment. Airborne contamination in a monolayer channel device monitored over a few months is shown in Fig. S4.† Similar to the 3-layer channel, the reduction in the flow over time through the channels could be revived by high temperature annealing (400 °C in H_2/Ar atmosphere). The difference observed in thick *versus* thin channel clogging could be related to the interaction strength between a hydrocarbon molecule and the channel surface under varying confinement. Even high temperature annealing (in combination with charcoal storage) is not efficient to revive the channels, implying a strong hydrocarbon-wall surface interaction inside thick channels. In the absence of the self-cleansing effect, thick channels might be decorated with polymeric residues inside channels, which may seed further adsorption of the hydrocarbons.

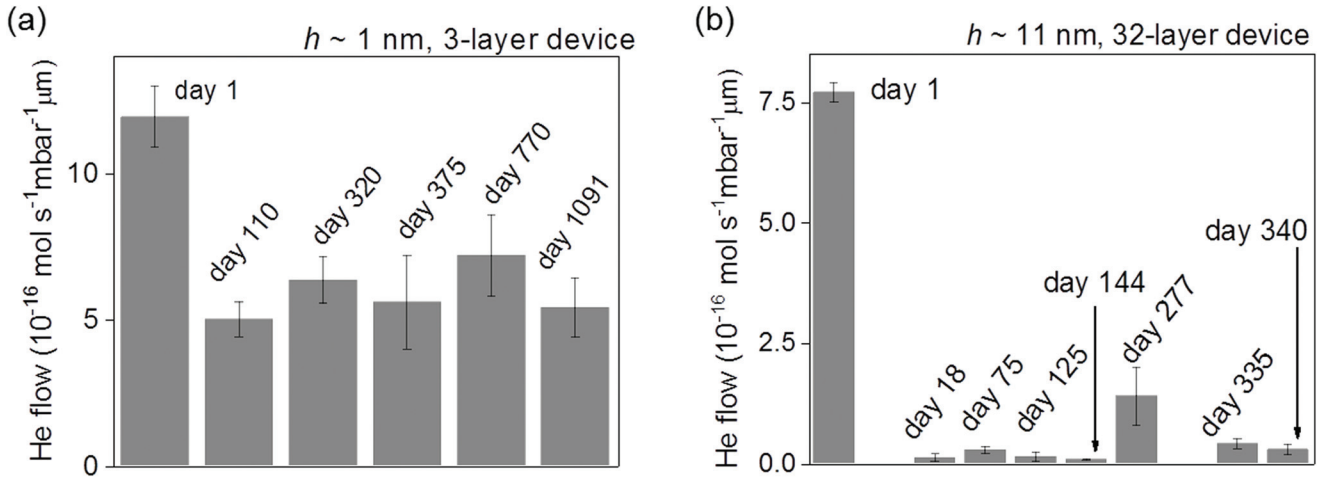

Fig. 2 He flow through Å-channel devices with heights, (a) $h \sim 1$ nm (3-layer graphene spacer) and (b) $h \sim 11$ nm (32-layer graphene spacer) monitored for over a duration of three years and one year, respectively. The bars represent He flows arbitrarily checked on different days through the same device when it was stored under charcoal. The devices were annealed before each measurement. Error bars are from two measurements on the same device.

Atmospheric hydrocarbons typically include a combination of several alkanes, volatile organic compounds such as alcohols, aldehydes, ethers, *etc*. In order to systematically probe the hydrocarbon molecule ingress into the channels, we chose hexane as a model molecule, due to three reasons, (1) it can be easily vaporized enabling experiments in the He flow measurement setup to monitor the effect of hexane exposure on the channels; (2) alkanes have relatively strong adsorption and can form close packed layers on the graphene and hBN basal surfaces due to the low potential energy and preferred orientation of carbons and hydrogens;[41] and (3) its kinetic diameter is small enough (~4.2 Å), which allows us to conveniently choose Å-slit channels which are smaller and larger than its size to investigate the contamination. We have custom made our He flow measurement set-up integrated with a hexane injector as depicted in Fig. S2.† By deliberately introducing the hexane, we examined the role of the height of the channels, in other words, the height of the confinement on the hydrocarbon contamination and the ease of channel clogging and unclogging. Within few seconds of the introduction of hexane into vacuum, a saturated pressure of ~200 mbar was achieved, implying that the hexane was in gas phase when approaching the nanochannels rather than the liquid form (Fig. S5†). Control experiments with an aperture of diameter ~60 nm showed that there was no unintended influence of hexane vapors on the measurement setup (further details in section S6†). Vaporized hexane is passed through the channels, and the gas conductance of He through channels was compared before and after hexane exposure (Fig. 3).

Hexane exposure and clogging of Å-slit channels of varying heights

To start with, we examined a five-layer graphite device ($h \sim$ 1.7 nm) deliberately exposed to hexane. Before introducing hexane, the channels showed a high helium flow $\sim 5.6 \times 10^{-15}$ mol s^{-1} $mbar^{-1}$ μm normalized per micron channel length and per mbar pressure difference (Fig. 3b). Upon introduction of hexane into the channels, the helium flow dropped more than three orders of magnitude going below the detection limit of the mass spectrometer. Let us note that the 5-layer channel (~1.7 nm) is large enough for hexane (kinetic diameter, ~0.42 nm) to enter. After the hexane was evacuated in the chamber, the following He measurement through the channels (first He flush) showed a distinct increase of the gas conductance occurring above ~100 mbar pressure (Fig. 3a). The revival of the channels continued with the second helium flush and stays at a stable gas conductance of $\sim 4 \times 10^{-15}$ mol s^{-1} $mbar^{-1}$ μm. A reduction of ~25% in the He flow relative to the pre-hexane exposure hints at a small portion of hexane remaining inside the channels. With further helium flushes, the adsorbed hexane could not be removed, indicating a limited unclogging efficiency of the helium flush method. Further desorption of hexane was done by a heat treatment of 150 °C for 20 minutes (purple curve in Fig. 3a), recovering the gas flow. Additional measurements of hexane exposure on graphite and hBN devices with the same channel heights are shown in ESI Fig. S7 and S8.† Let us note that the striking behaviour of the recovery, the steps of increased gas flow in a dynamic fashion after the first He flush (blue scatter in Fig. 3a), is not captured in other devices with the same channel height (in Fig. S7 and S8†). Probably, the revival process is transient and may depend on several factors that it cannot be experimentally recorded every time.

Next, we investigated hexane contamination when the hexane molecule size is comparable to the channel size, in this case, the bilayer channel device ($h \sim 0.7$ nm). To our surprise, a complete blockage is caused by hexane and we cannot revive the channels either by helium flushes or by heating (Fig. 3c and d). Further annealing at high temperatures also did not achieve the revival. We performed the same experi-

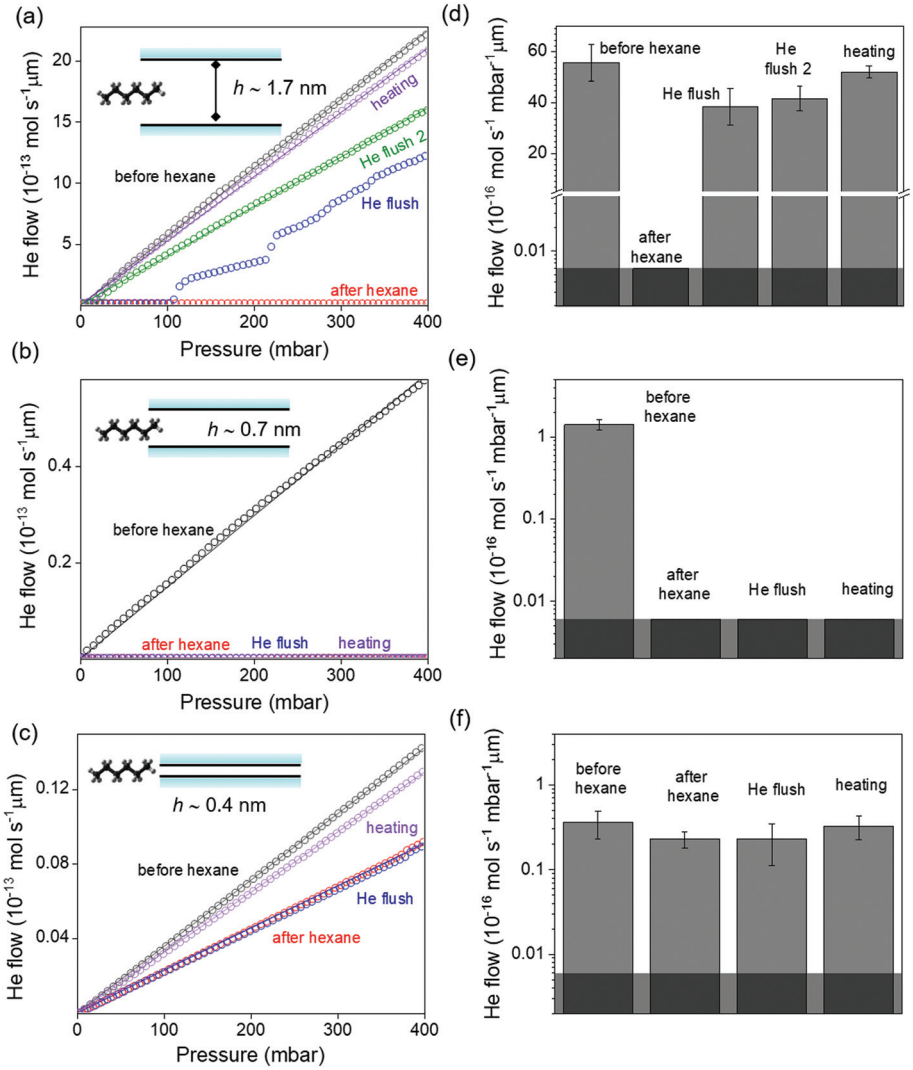

Fig. 3 Comparison of helium leak rate before and after exposure to hexane through various graphite Å-channel devices with heights, (a) $h \sim 1.7$ nm, (b) $h \sim 0.7$ nm, and (c) $h \sim 0.4$ nm. The insets show the schematics depicting the relative size of the hexane molecule to the channel in each case. The bar graphs in (b), (d) and (f) are obtained from (a), (c) and (e) and represent normalized He flow per unit pressure. Grey shaded area indicates the limit of detection. All the graphs represent the flows normalized per single channel and per μm length of the channel. Error bars are from two measurements on the same device, and where there was only measurement (*e.g.*, He flush), it represents uncertainty in the best fit to the measured data.

ment on monolayer channels ($h \sim 0.4$ nm) which are thinner than the size of the hexane molecule. An initial He conductance of a monolayer channel of $\sim 2.2 \times 10^{-17}$ mol s^{-1} mbar^{-1} μm reduced to about $\sim 2 \times 10^{-17}$ mol s^{-1} mbar^{-1} μm upon exposure to hexane, and it can be totally revived by heating (Fig. 3e and f).

The effect of channel height on the interaction of hexane in the Å-slit channels

Let us discuss the plausible reasons behind the observed phenomenon. Given the size of hexane, it is reasonable to expect it to be rejected from entering the monolayer channels due to the size restriction, as observed in experiments. It has to be noted that monolayer channels possess clean surfaces due to the proximity of the top and bottom layers, expelling the contaminants outside from the self-cleansing effect,[37] and can hinder the hydrocarbons from entering. The small reduction in the flow observed for the monolayer channels after exposure to hexane could be possibly due to the trace layer of hexane on the entry blocking the He, and this was easily revived by flushing and heat treatment. With respect to the bilayer channels, they have a relatively close size match between the hexane molecule kinetic diameter and channel height, which could lead to a tight confinement imposing a strong interaction of the channel walls with the long alkyl chain. We observed similar trends using channels with hBN walls (gas flow measurements shown in Fig S8†). Let us recall that this principle of close size match between molecules and

the pores is explored for preferred adsorption of water and hydrocarbons, in capillary condensation at lower than saturation pressures into molecular sieves,[42] hydrogen capture into porous systems,[43] and activated carbon for the removal of volatile organic compounds.[44]

The ease of clogging and unclogging of channels with varying heights differs and can be largely linked to the strength of the hydrocarbon molecule-surface interaction. Further theoretical studies are required to quantitatively analyze the interaction strength. Here our experimental methods for removing hexane through helium flush and heat treatment can qualitatively compare the hydrocarbon–nanochannel interactions. Helium flush could slightly remove the adsorbed hexane molecules but with limited effect. On the other hand, by heating the freshly clogged devices to 150 °C, we could revive the channels by desorbing the adsorbed hexane. Those channels (h > 2 nm) which can hardly be recovered by heating to 150 °C may contain a strong interaction developed between the hydrocarbons and the channel surface. Additionally, the severity of clogging increased with time, as can be seen from the airborne contamination discussed in Fig. 1 and Fig. 2. Thermal annealing at high temperatures has been reported by several groups to decontaminate/desorb hydrocarbons on surfaces of 2D materials, which we also observed here for Å-channels. When the channel size is much larger (*e.g.*, in the case of $h \sim 11$ nm), it proved difficult to revive the pores which may indicate the possible formation of hydrocarbon and polymeric clusters which can interact with the channel surface rather than the molecular-level interaction of hydrocarbons.

Conclusions

In conclusion, we report the influence of hydrocarbons in a confined channel and discuss the clogging and revival by intentionally exposing hydrocarbon contaminants into the nanochannels. Our experiments highlight that the confining dimension (*i.e.*, channel height in the slits) has a dispensable effect on the severity of hydrocarbon contamination. The monolayer channel shows a robust stability which can be attributed to its clean surfaces. In contrast, a vigorous confinement from the channel with a size closely matching that of the molecular size of the hydrocarbons results in a strengthened surface adsorption, making the recovery and decontamination highly difficult. Examining the hydrocarbon contamination which can lead to channel clogging, and revival methods for unclogging as discussed here, can benefit several applications of membranes such as water desalination and gas separation in assessing pore cleanliness and stability.

Experimental section

Fabrication of Å-slit channels

We fabricated the Å-slit channels by vertically stacking 2D crystals over each other in a layer-by-layer fashion as reported previously[38] (the detailed fabrication process flow is given in ESI Fig. S1†). The device is composed of three layers. The bottom and top 2D crystals in the fabrication of channel devices are chosen to be either graphite or hBN whereas the spacer 2D crystals are always monolayer or few layer thick graphene. The fabrication began with making a free-standing SiN_x membrane (~100 μm × 100 μm) supported over a Si substrate. With an additional photolithography step and a reactive ion etching, a rectangular hole of 3 μm × 25 μm was then made on the SiN_x membrane. The bottom, spacer and top layers were transferred one over the other to cover the hole. The spacer layer is typically made up of ~130 (±10) nm wide graphene strips with a ~130 (±10) nm separation using electron-beam lithography and oxygen plasma etching. A gold patch was made over the tricrystal stack to prevent the sagging of top crystal thin edges into the channels and to use it as a mask to define the channel length. Thus, a 2D channel is made in the tri-crystal stack where the channel length (L) is defined by the edge of the metal mask to the edge of the rectangular hole, the channel width (w) in our channels is always 130 nm, and the channel height (h) is defined by the spacer 2D crystal thickness (mono- to few layer thick graphene). The channel width and height were acquired using atomic force microscopy (AFM) (Fig. S9†). The AFM images of spacer strips show their cleanliness, and it is a checkpoint to select suitable spacers which are used further for channel fabrication (Fig. S9 and Table S1†). After the transfer of each layer, the Å-channel devices were annealed in a furnace at 400 °C for 4 hours under a flow of H_2/Ar gas mixture. The devices were stored in activated charcoal; please see ESI S3† for further details about storage.

Cross-sectional imaging of Å-slit channels

For the cross-sectional imaging, thin cross-sectional lamellae were prepared using an *in situ* lift-out procedure. Perpendicular to the Å-slits' axis, lamellae were cut by high-precision site-specific milling in Helios Nanolab DualBeam 660, incorporating both a scanning electron microscope and focused ion-beam columns. To weld the lamella to a micromanipulator, platinum was deposited using the ion beam, enabling its lift-off from the substrate. After transferring to a specialist OmniProbe TEM grid, the lamellae were further thinned to less than 100 nm and polished to electron transparency, using 5 kV and subsequently 2 kV ion milling. High-resolution STEM and HAADF images were acquired with an aberration-corrected microscope (FEI Titan G2 80–200 kV) using a probe convergence angle of 21 mrad, a HAADF inner angle of 48 mrad and a probe current of about 70 pA. The electron beam was aligned parallel to the Å-slits, using the relevant Kikuchi bands of the silicon substrate and the assembled 2D crystals.

Helium flow measurement

We measure helium gas flows through the nanochannels to verify the clogging and unclogging of the channels, using a helium leak detector, and the schematic of the setup is

depicted in ESI Fig. S2.† It is a two-chamber assembly where one chamber is connected to a voltage control valve to alter helium gas flow, a pressure gauge, a scroll pump to evacuate the system, and a hydrocarbon injecting valve with a Swagelok that allows the introduction of hexane into the system. The Å-slit channel device is clamped in a customised sample holder which is then held between the two chambers and secured with vacuum O-rings, such that the channels are the only pathway for mass transport. Both ends of the sample holder are connected to the scroll pump that helps to maintain the chambers in a vacuum down to 10^{-2} mbar. Through a valve, the helium gas was let into the top chamber and it permeated through the Å-slit channels to reach the bottom chamber which was connected to a mass spectrometer (INFICON UL200) to measure the flow rate of helium gas. All the measurements were conducted at room temperature of 298 K. For further details about the measurement setup, please refer to ESI S2.†

To evaluate the helium measurement setup, we conducted several trials on control substrates which are blank SiN_x/Si wafers, and the reference devices with SiN_x membranes have a tri-crystal stack but without any channels in the spacer layer. There is no notable helium flow in both control and reference devices proving that the system is well-sealed.

Channel reviving process

In this study, we employed three methods to unclog the channels. One is the helium flushing method in which the chamber above the entrance of the channel is filled with helium gas of ~1 bar whereas the exit side of the channel faces vacuum. By continuous flushing for 10 minutes, the helium gas could revive the channels. The second one is a heating process where the device is placed on a hot plate and heated at 150 °C for 20 minutes to desorb the hexane. While the above two were used in the case of deliberate exposure of channels to hexane, the third method of high temperature annealing in 10% H_2/argon at 400 °C for 4 hours was done for routine cleaning of channels from both airborne contamination and during fabrication to remove polymer residues.

Author contributions

B. R. designed and directed the project. A. K. and Y. Y. fabricated and characterized the devices. R. Q. characterized the spacers. A. R. and S. H provided STEM measurements. R. S. and S. G. conducted gas measurements. R. S., S. G., and A. B. analyzed airborne contamination data. R. S., A. K., and B. R. performed hexane contamination experiments and analysis. Y. Y., B. R., and A. K. wrote the manuscript with inputs from R. S. All authors contributed to discussions.

Conflicts of interest

The authors declare that there are no conflicting interests.

Acknowledgements

B. R. acknowledges the funding from the European Union's H2020 Framework Programme/ERC Starting Grant Agreement no. 852674 – AngstroCAP, Royal Society University Research Fellowship URF\R1\180127 and enhancement award RGF\EA \181000, EPSRC Grant EP/R013063/1. A. K. acknowledges the Ramsay Memorial Fellowship, the Royal Society research grant RGS\R2\202036.

References

1 L. Bocquet, *Nat. Mater.*, 2020, **19**, 254–256.
2 S. P. Koenig, L. Wang, J. Pellegrino and J. S. Bunch, *Nat. Nanotechnol.*, 2012, **7**, 728–732.
3 S. Howorka and Z. Siwy, *Chem. Soc. Rev.*, 2009, **38**, 2360–2384.
4 J. Feng, M. Graf, K. Liu, D. Ovchinnikov, D. Dumcenco, M. Heiranian, V. Nandigana, N. R. Aluru, A. Kis and A. Radenovic, *Nature*, 2016, **536**, 197–200.
5 D.-e. Jiang, V. R. Cooper and S. Dai, *Nano Lett.*, 2009, **9**, 4019–4024.
6 X. Yang, C. Cheng, Y. Wang, L. Qiu and D. Li, *Science*, 2013, **341**, 534–537.
7 M. Majumder, N. Chopra, R. Andrews and B. J. Hinds, *Nature*, 2005, **438**, 44–44.
8 R. H. Tunuguntla, F. I. Allen, K. Kim, A. Belliveau and A. Noy, *Nat. Nanotechnol.*, 2016, **11**, 639–644.
9 R. R. Nair, H. A. Wu, P. N. Jayaram, I. V. Grigorieva and A. K. Geim, *Science*, 2012, **335**, 442–444.
10 J.-J. Shao, K. Raidongia, A. R. Koltonow and J. Huang, *Nat. Commun.*, 2015, **6**, 7602.
11 B. Anasori, M. R. Lukatskaya and Y. Gogotsi, *Nat. Rev. Mater.*, 2017, **2**, 16098.
12 J. P. Thiruraman, K. Fujisawa, G. Danda, P. M. Das, T. Zhang, A. Bolotsky, N. Perea-López, A. Nicolaï, P. Senet, M. Terrones and M. Drndić, *Nano Lett.*, 2018, **18**, 1651–1659.
13 S. P. Surwade, S. N. Smirnov, I. V. Vlassiouk, R. R. Unocic, G. M. Veith, S. Dai and S. M. Mahurin, *Nat. Nanotechnol.*, 2015, **10**, 459–464.
14 L. Wang, M. S. H. Boutilier, P. R. Kidambi, D. Jang, N. G. Hadjiconstantinou and R. Karnik, *Nat. Nanotechnol.*, 2017, **12**, 509–522.
15 N. Kavokine, R. R. Netz and L. Bocquet, *Annu. Rev. Fluid Mech.*, 2021, **53**, 377–410.
16 A. Nourbakhsh, M. Cantoro, A. Klekachev, F. Clemente, B. Sorée, M. H. van der Veen, T. Vosch, A. Stesmans, B. Sels and S. De Gendt, *J. Phys. Chem. C*, 2010, **114**, 6894–6900.
17 A. Kozbial, F. Zhou, Z. Li, H. Liu and L. Li, *Acc. Chem. Res.*, 2016, **49**, 2765–2773.
18 Z. Li, Y. Wang, A. Kozbial, G. Shenoy, F. Zhou, R. McGinley, P. Ireland, B. Morganstein, A. Kunkel, S. P. Surwade, L. Li and H. Liu, *Nat. Mater.*, 2013, **12**, 925–931.
19 T. Fujimoto, K. Takeda and T. Nonaka, in *Developments in Surface Contamination and Cleaning*, ed. R. Kohli and

K. L. Mittal, William Andrew Publishing, Norwich, NY, 2008, pp. 329–474.
20 P. K. Chow, E. Singh, B. C. Viana, J. Gao, J. Luo, J. Li, Z. Lin, A. L. Elías, Y. Shi, Z. Wang, M. Terrones and N. Koratkar, *ACS Nano*, 2015, **9**, 3023–3031.
21 X. Chen, Z. Yang, S. Feng, T. W. Golbek, W. Xu, H.-J. Butt, T. Weidner, Z. Xu, J. Hao and Z. Wang, *Nano Lett.*, 2020, **20**, 5670–5677.
22 E. Khestanova, F. Guinea, L. Fumagalli, A. K. Geim and I. V. Grigorieva, *Nat. Commun.*, 2016, **7**, 12587.
23 S. J. Haigh, A. Gholinia, R. Jalil, S. Romani, L. Britnell, D. C. Elias, K. S. Novoselov, L. A. Ponomarenko, A. K. Geim and R. Gorbachev, *Nat. Mater.*, 2012, **11**, 764–767.
24 G. Algara-Siller, O. Lehtinen, A. Turchanin and U. Kaiser, *Appl. Phys. Lett.*, 2014, **104**, 153115.
25 Z. Cheng, Q. Zhou, C. Wang, Q. Li, C. Wang and Y. Fang, *Nano Lett.*, 2011, **11**, 767–771.
26 J.-N. Longchamp, C. Escher and H.-W. Fink, *J. Vac. Sci. Technol.*, 2013, **31**, 020605.
27 L. F. Villalobos, S. Huang, M. Dakhchoune, G. He, W.-C. Lee and K. V. Agrawal, *Carbon*, 2020, **173**, 980–988.
28 D. E. Starr, Z. Liu, M. Hävecker, A. Knop-Gericke and H. Bluhm, *Chem. Soc. Rev.*, 2013, **42**, 5833–5857.
29 C. A. Amadei, C.-Y. Lai, D. Heskes and M. Chiesa, *J. Chem. Phys.*, 2014, **141**, 084709.
30 C.-Y. Lai, T.-C. Tang, C. A. Amadei, A. J. Marsden, A. Verdaguer, N. Wilson and M. Chiesa, *Carbon*, 2014, **80**, 784–792.
31 A. Dazzi and C. B. Prater, *Chem. Rev.*, 2017, **117**, 5146–5173.
32 M. Koshino, N. Solin, T. Tanaka, H. Isobe and E. Nakamura, *Nat. Nanotechnol.*, 2008, **3**, 595–597.
33 J. C. Meyer, F. Eder, S. Kurasch, V. Skakalova, J. Kotakoski, H. J. Park, S. Roth, A. Chuvilin, S. Eyhusen, G. Benner, A. V. Krasheninnikov and U. Kaiser, *Phys. Rev. Lett.*, 2012, **108**, 196102.
34 J. Li, Q. Rao, Y. Xia, M. Hoepfner and M. D. Deo, *Langmuir*, 2020, **36**, 7277–7288.
35 H. Qu, A. Rayabharam, X. Wu, P. Wang, Y. Li, J. Fagan, N. R. Aluru and Y. Wang, *Nat. Commun.*, 2021, **12**, 310.
36 Y.-C. Lin, C.-C. Lu, C.-H. Yeh, C. Jin, K. Suenaga and P.-W. Chiu, *Nano Lett.*, 2012, **12**, 414–419.
37 A. Keerthi, A. K. Geim, A. Janardanan, A. P. Rooney, A. Esfandiar, S. Hu, S. A. Dar, I. V. Grigorieva, S. J. Haigh, F. C. Wang and B. Radha, *Nature*, 2018, **558**, 420–424.
38 B. Radha, A. Esfandiar, F. C. Wang, A. P. Rooney, K. Gopinadhan, A. Keerthi, A. Mishchenko, A. Janardanan, P. Blake, L. Fumagalli, M. Lozada-Hidalgo, S. Garaj, S. J. Haigh, I. V. Grigorieva, H. A. Wu and A. K. Geim, *Nature*, 2016, **538**, 222–225.
39 A. Kozbial, Z. Li, J. Sun, X. Gong, F. Zhou, Y. Wang, H. Xu, H. Liu and L. Li, *Carbon*, 2014, **74**, 218–225.
40 B. Ramos-Alvarado, *J. Chem. Phys.*, 2019, **151**, 114701.
41 A. J. Groszek and E. K. Rideal, *Proc. R. Soc. London, Ser. A*, 1970, **314**, 473–498.
42 S. Sircar and A. L. Myers, in *Handbook of Zeolite Science and Technology*, ed. S. M. Auerbach, K. A. Carrado and P. K. Dutta, CRC Press New York, 2003.
43 Y. Gogotsi, C. Portet, S. Osswald, J. M. Simmons, T. Yildirim, G. Laudisio and J. E. Fischer, *Int. J. Hydrogen Energy*, 2009, **34**, 6314–6319.
44 Y. An, Q. Fu, D. Zhang, Y. Wang and Z. Tang, *Chemosphere*, 2019, **227**, 9–16.